

**Millimeter-wave  
stratocumulus LWP  
retrievals**

P. Zuidema et al.

This discussion paper is/has been under review for the journal Atmospheric Chemistry and Physics (ACP). Please refer to the corresponding final paper in ACP if available.

# Aircraft millimeter-wave retrievals of cloud liquid water path during VOCALS-REx

P. Zuidema<sup>1</sup>, D. Leon<sup>2</sup>, A. Pazmany<sup>3</sup>, and M. Cadetdu<sup>4</sup>

<sup>1</sup>Rosenstiel School of Marine and Atmospheric Sciences, Univ. of Miami, Miami, Florida, USA

<sup>2</sup>Department of Atmospheric Sciences, University of Wyoming, Laramie, Wyoming, USA

<sup>3</sup>Prosensing Inc., Amherst, Massachusetts, USA

<sup>4</sup>Argonne National Laboratory, Argonne, Illinois, USA

Received: 2 July 2011 – Accepted: 4 July 2011 – Published: 8 July 2011

Correspondence to: P. Zuidema (pzuidema@rsmas.miami.edu)

Published by Copernicus Publications on behalf of the European Geosciences Union.

Title Page

Abstract

Introduction

Conclusions

References

Tables

Figures

◀

▶

◀

▶

Back

Close

Full Screen / Esc

Printer-friendly Version

Interactive Discussion



## Abstract

A unique feature of the VOCALS Regional Experiment was the inclusion of a small, inexpensive, zenith-pointing millimeter-wavelength passive radiometer on the fourteen research flights of the NCAR C-130 plane, the G-band (183 GHz) Vapor Radiometer (GVR). The radiometer permitted above-cloud retrievals of water vapor path, and cloud liquid water path retrievals at 1 Hz resolution for the sub-cloud and cloudbase aircraft legs when combined with in-situ thermodynamic data. Retrieved free-tropospheric (above-cloud) water vapor paths possessed a strong longitudinal gradient, with off-shore values of one to two mm and near-coastal values reaching one cm. Overall the free-troposphere was drier than that sampled by radiosondes in previous years. For the sub-cloud legs, the absolute (between-leg) and relative (within-leg) LWP accuracy was estimated at 20–25 and 5 g m<sup>-2</sup> respectively for well-mixed conditions, with greater uncertainties expected for decoupled conditions. Clouds with retrieved liquid water paths between 200 to 400 g m<sup>-2</sup> matched adiabatic values derived from coincident cloud thickness measurements exceedingly well. A significant contribution of the GVR dataset is the extended information on the thin clouds, with 66 % of the retrieved LWPs < 100 g m<sup>-2</sup>. Nevertheless, the overall LWP cloud fraction of 62 % was less than the 92 % cloud cover determined by airborne cloud lidar and radar combined.

## 1 Introduction

Cloud liquid water and its distribution are a first-order climate impact of marine stratocumulus regions. Microwave radiometry has contributed to this radiative assessment by providing oceanic cloud liquid water path (LWP) measurements from space, island, ship, and aircraft platforms (e.g., O'Dell et al., 2008; Seethala and Horvath, 2010; Wood et al., 2002; Cahalan et al., 1994; Liu et al., 2003; Zuidema et al., 2005). These have been used to assess model cloud process depictions at a variety of scales (e.g., Siebesma et al., 2004; Zhu et al., 2005; Bennartz et al., 2011; Wood et al., 2009).

### Millimeter-wave stratocumulus LWP retrievals

P. Zuidema et al.

Title Page

Abstract

Introduction

Conclusions

References

Tables

Figures



Back

Close

Full Screen / Esc

Printer-friendly Version

Interactive Discussion



Microwave LWPs, because they are derived independently of optical techniques, have also aided aerosol indirect effect assessments (e.g., McComiskey et al., 2009, and references therein). In one airborne application, data from the downward-scanning Airborne Imaging Microwave Radiometer were combined with reflectance measurements to assess aerosol susceptibility over the Indian Ocean (Liu et al., 2003).

A unique feature of the VOCALS Regional Experiment was the inclusion upon the NCAR C-130 airplane of a small (fitting into a standard microphysical probe canister), inexpensive, zenith-pointing millimeter-wavelength passive radiometer, the G-band Vapor Radiometer (GVR) (Pazmany, 2006). The zenith view of a stable cold space background eases the LWP retrievals. The GVR-retrieved LWP data have the potential to expand our ability to characterize stratocumulus clouds, their cloud-aerosol interactions and precipitation dynamics. The GVR was originally intended for Arctic research because of the high sensitivity of 170–197 GHz emission to low amounts of water vapor and liquid water (i.e., precipitable water vapor paths <5 mm). For stratocumulus regions, millimeter-wave radiometers may be particularly valuable for thin clouds that are difficult for a cloud radar to sense.

A GVR was placed within one of the standard NCAR C-130 microphysical probes during VOCALS-REx. The C-130 flight plans, of which an example is shown in Fig. 1, included sub-cloud legs (~150 m altitude), cloud-base legs at times, and above-cloud legs (~1370 m altitude), of 10 or 40 min duration (see Wood et al. (2011b) for more detail). Cloud liquid water paths could be retrieved during the sub-cloud and cloud-base legs at a 1 Hz sampling rate, and free-tropospheric water vapor paths retrieved during the above-cloud legs. This was the first field experiment focused on subtropical stratocumulus to include millimeter-wave radiometers (another radiometer of different design and calibration technique, the Radiometrics MP-183, was simultaneously deployed upon the R/V *Ron Brown*). The utility of millimeter-wave radiometers for stratocumulus process studies thus needs to be established. The purpose of this paper is to do so for the airborne GVR.

## Millimeter-wave stratocumulus LWP retrievals

P. Zuidema et al.

Title Page

Abstract

Introduction

Conclusions

References

Tables

Figures

◀

▶

◀

▶

Back

Close

Full Screen / Esc

Printer-friendly Version

Interactive Discussion



## 2 The southeast Pacific radiative environment

A surface-based version of the GVR was deployed at Barrow, Alaska (Pazmany, 2006; Cadeddu et al., 2007; Cimini et al., 2007, 2009; Racette et al., 2005), where the high sensitivity of 170–197 GHz radiation to water vapor and liquid water emission within a cold, dry climate could be used to full advantage. For the more moist southeast Pacific stratocumulus region, the sensitivity available for discriminating liquid water from water vapor at wavelengths around 183 GHz depends significantly on the water vapor path. Initial expectations were developed from radiosondes released during seven buoy-tending cruises occurring from the year 2001 through 2008. All but two of the cruises took place in October, and all spent the majority of their time along the 20° S line out to the 85° W (see Zuidema et al. (2009) and de Szoeké et al. (2010) for further description). Histograms of the water vapor paths (WVPs) for the years prior to VOCALS-REx and separately for the VOCALS cruise are shown in Fig. 2. Free-tropospheric (at 1370 m altitude) WVPs during VOCALS-REx were low compared to other years, typically < 0.5 mm with outliers up to three mm. These WVPs are similar to surface WVP values for Barrow, Alaska (Turner and Mlawer, 2010), and reinforce the idea that a broad window in the infrared spectrum is available for stratocumulus cloud top radiative cooling in the southeast Pacific. Water vapor paths calculated from a reference altitude of 150 m, representative of the aircraft sub-cloud legs, show VOCALS-REx WVPs ranging between eight to twenty mm (Fig. 2b), also lower than for other years.

The several hundreds of Vaisala RS-90 series radiosonde profiles from four different Octobers in the southeast Pacific were used to advantage within the retrieval process. Brightness temperatures calculated from such radiosondes compared well to Arctic GVR measurements (Payne et al., 2008) and to chilled mirror hygrometers (Miloshevich et al., 2006), particularly during nighttime (Miloshevich et al., 2009). We used a best-fit of the GVR measurements to forward-calculated brightness temperatures from the radiosondes to retrieve WVP and LWP. The GVR measures brightness temperatures

### Millimeter-wave stratocumulus LWP retrievals

P. Zuidema et al.

Title Page

Abstract

Introduction

Conclusions

References

Tables

Figures



Back

Close

Full Screen / Esc

Printer-friendly Version

Interactive Discussion



from four double-sideband channels, centered at  $\pm 1$ ,  $\pm 3$ ,  $\pm 7$ , and  $\pm 14$  GHz off of the 183.31 GHz water vapor absorption line (Pazmany, 2006). Downwelling brightness temperatures ( $T_b$ s) were simulated using the 10th and 90th percentile of the 330 Vaisala RS-92 radiosondes reaching 50 hPa that were launched over the southeast Pacific stratocumulus region. The simulated brightness temperatures are shown for the 0–220 GHz frequency range (Fig. 3, bottom panel, black and red solid lines respectively), and for the 165–200 GHz range (top panel). The spectra corresponding to the above-cloud legs (purple and yellow lines) show the center lines retaining their sensitivity to moisture. The spectra representative of the subcloud legs (red and black lines) show that fully saturated center absorption lines. Nevertheless, the wing lines retain a strong sensitivity to liquid water path regardless of WVP.

The response of the GVR  $T_b$ s to liquid water diminishes as the water vapor path increases. The sensitivity of the two outer wing line  $T_b$ s to liquid water path is shown in more detail in Fig. 4. The  $\pm 7$  GHz lines (red lines) lose sensitivity to cloud liquid water path in more moist conditions, while the outer wing lines ( $\pm 14$  GHz, black lines) remain responsive to liquid water regardless of the water vapor path. For this reason, the  $\pm 14$  GHz GVR channel alone was chosen against which to measure a best-fit of forward-calculated radiosonde  $T_b$ s for the LWP retrieval. The outer wing lines combined have  $\frac{\delta T_b}{\delta LWP}$  sensitivities ranging between 0.6 K–1.5 K per  $10 \text{ g m}^{-2}$  depending on water vapor. For a LWP of  $100 \text{ g m}^{-2}$ , an undetected change in WVP of 0.2 mm would create a  $T_b$  error of almost 1 K – equivalent to a LWP change of  $6\text{--}10 \text{ g m}^{-2}$ .

### 3 Above-cloud water vapor paths

Free-tropospheric water vapor paths were retrieved using all four channels during the above-cloud legs (with the altitude recorded). As expected for a strongly-subsiding atmosphere, the off-shore free-tropospheric WVP did not typically vary much over the distance of one leg (about 72 km). Usually one leg-mean water vapor path value represented the whole leg adequately. Near the coast, continental moisture outflow could give rise to gradients in the measured  $T_b$ s.

## Millimeter-wave stratocumulus LWP retrievals

P. Zuidema et al.

Title Page

Abstract

Introduction

Conclusions

References

Tables

Figures



Back

Close

Full Screen / Esc

Printer-friendly Version

Interactive Discussion



**Millimeter-wave  
stratocumulus LWP  
retrievals**

P. Zuidema et al.

Title Page

Abstract

Introduction

Conclusions

References

Tables

Figures

◀

▶

◀

▶

Back

Close

Full Screen / Esc

Printer-friendly Version

Interactive Discussion



The above-cloud WVPs are interesting in themselves through providing another insight into the subsiding free-troposphere. They are also useful for assessing instrument and retrieval performance in a simpler clear-sky radiative environment. In the next four subsections, the instrument calibration is discussed first, then the millimeter-wave absorption models along with the full range of radiosonde-calculated values shown and GVR  $T_{bs}$  from one above-cloud leg. Next a comparison between the GVR measurements and sonde-calculated values is shown for one sonde launched near-in-time from the R/V *Ron Brown*. Last, the above-cloud WVPs from all fourteen research flights are compiled and compared against those from radiosondes from both 2008 and previous years.

### 3.1 Instrument calibration

An independent, external calibration was done immediately prior to VOCALS-REX using a foam of known emissivity. During the field deployment, the GVR calibrated itself operationally using internal warm and hot loads on a continuous cycle lasting ten seconds. The absolute calibration was estimated to be  $\sim 2$  K based on comparisons of the ground GVR to radiosondes and other millimeter-wave radiometers at Barrow, Alaska (Cadeddu et al., 2007; Cimini et al., 2009). The temporal resolution of the reported brightness temperatures was set to approximately 1 second, to be on a common framework with that of other remote sensing measurements. The relative calibration (i.e., the accuracy of individual values compared to their neighbors) over a one second time interval is estimated to be  $< 0.5$  K from Fig. 3 of Pazmany (2006) for the least-stable outer wing line brightness temperature. As can be deduced from Fig. 4, a 2 K absolute and 0.5 K relative instrument accuracy is equivalent to an absolute LWP uncertainty of between  $10$ – $20$   $\text{g m}^{-2}$ , and a relative LWP uncertainty  $< 5$   $\text{g m}^{-2}$  for a dry environment, decreasing with LWP. Noise induced by thermal instability from instrument heating, which may have been a factor during the daytime flights, is not accounted for in this estimate. Other details on the calibration can be found in Cadeddu et al. (2007).

### 3.2 Millimeter-wavelength absorption models

The correspondence between sonde-calculated  $T_b$ s and the GVR measurements also depends on the microwave absorption models used to convert radiosonde moisture and temperature profiles into microwave brightness temperature values. Recent assessments of gaseous absorption models at millimeter frequencies include Hewison (2006), Payne et al. (2008) and Turner et al. (2009). Previous efforts to retrieve LWP using all four channels found values that were markedly smaller than those using 22–30 GHz retrievals (Cadeddu et al., 2007), with Payne et al. (2008) implying issues with the spectroscopic specification of the 183 GHz absorption line. Previous work in this stratocumulus region (Zuidema et al., 2005) favored the Liljegren et al. (2005) gaseous absorption model, itself modified from Rosenkranz (1998). For the VOCALS-REx retrievals we further modified the Liljegren et al. (2005) gaseous absorption model to include the water vapor continuum coefficients in Table IV of Turner et al. (2009). This modification brings intermodel differences to within 2K over the window regions between 10 to 400 GHz Turner et al. (2009), most applicable to the  $\pm 7$  and  $\pm 14$  wing lines for which the water vapor continuum specification contributes more to the  $T_b$  than the absorption line specification.

The GVR liquid water path calculations also relied on the Liebe et al. (1991) and Liebe et al. (1993) liquid dielectric models. Water permittivity models are more difficult to evaluate because of a lack of independent measurements of liquid water path, but the Liebe et al. (1993) model produced results similar to that of other models in the 10°C–20°C temperature range (Cadeddu and Turner, 2011). The more important limitation is that all of our calculations assumed Rayleigh scattering and attenuation; at the radiometer wavelength of  $\sim 1.66$  mm, Mie scattering and attenuation effects can be large within heavy stratocumulus precipitation, if partially compensating for each other.

Calculations for this study were monochromatic. A climatological sounding for the stratosphere was extrapolated onto the radiosonde soundings; previous studies concluded that the uncertainty in the water vapor specification above 10 km was

## Millimeter-wave stratocumulus LWP retrievals

P. Zuidema et al.

Title Page

Abstract

Introduction

Conclusions

References

Tables

Figures

◀

▶

◀

▶

Back

Close

Full Screen / Esc

Printer-friendly Version

Interactive Discussion



insignificant (Cadeddu et al., 2007; Payne et al., 2008). In addition, although in theory the millimeter-wave  $T_b$ s could be increased by scattering from high-altitude ice crystals, the observed cirrus fraction was low and clouds thin. We have not accounted for any contribution of cirrus to the measured  $T_b$ s.

The full range of radiosonde-calculated  $T_b$ s at 1370 m altitude is shown in Fig. 5. The  $T_b$  response to increasing WVP was mostly linear for the wing lines, while the center line demonstrated a non-linear response as WVPs increased beyond 2 mm. The spread in the  $T_b$  values at a given WVP indicated sensitivity to the water vapor vertical profile and its emission temperature at those heights (Racette et al., 2005). Most free-tropospheric moisture variability occurred at  $\sim 5$  km and in the upper troposphere (Fig. 6).

The correspondence of GVR measurements for a nighttime near-coastal 21 October flight leg (RF3 AC1) to the forward-calculated values is also shown in Fig. 5. The  $\pm 3$  GHz line demonstrated the strongest sensitivity to WVPs between 1 to 3.5 mm, maintained the most linear response, and was the most tightly constrained of the four channels (Fig. 5). If an initial WVP estimate were made using a best-fit to the  $\pm 3$  GHz line only, the deviations from the other channels can suggest an error estimate. We estimated a conservative error estimate of  $\sim 0.2$  mm this way for the example shown in Fig. 5, though all four channels provided a reasonable fit to the simulated  $T_b$ s, equivalent to the radiative signature of  $6\text{--}8$  g m $^{-2}$  of liquid water (Fig. 4).

### 3.3 Comparison to R/V *Ron Brown* sonde

Another assessment of each of the GVR channel measurements, and the overall calibration, can be done by comparing GVR  $T_b$ s to those calculated from soundings released nearby from the R/V *Ronald H. Brown*. Of the three C-130 overflights of the ship (25 October (RF5), 2 November (RF8), and 11 November (RF12)), only the 2 November overflight occurred during the night, freeing the comparison from a known dry daytime humidity bias of about 5% (Miloshevich et al., 2009). The comparison for 2 November is shown in Fig. 7. The two aircraft above-cloud legs occurred 18 min prior and 41 min after a sounding was launched, approximately 100 km east and 50 km west of the ship.

## Millimeter-wave stratocumulus LWP retrievals

P. Zuidema et al.

Title Page

Abstract

Introduction

Conclusions

References

Tables

Figures

◀

▶

◀

▶

Back

Close

Full Screen / Esc

Printer-friendly Version

Interactive Discussion



**Millimeter-wave  
stratocumulus LWP  
retrievals**

P. Zuidema et al.

Title Page

Abstract

Introduction

Conclusions

References

Tables

Figures

◀

▶

◀

▶

Back

Close

Full Screen / Esc

Printer-friendly Version

Interactive Discussion



The GVR-estimated WVPs from the above-cloud legs were respectively 2.0 mm and 1.5 mm (at 1.38 and 1.60 km altitude), while the radiosonde-derived values were 1.42 and 1.27 mm – i.e., the GVR-retrieved WVPs exceeded radiosonde values by 0.6 and 0.2 mm respectively. The eastern flight leg did show a longitudinal  $T_b$  gradient, which if extrapolated, may explain some of the 0.6 mm discrepancy.

A comparison using 11 November overflight data also showed the GVR  $T_b$ s exceeding the radiosonde-calculated values, most noticeable for the center lines. The overflight occurred during the afternoon, but exceeded the 5% estimated from solar absorption (Miloshevich et al., 2006). For both 2 November and 11 November cases, the comparison at  $\pm 3$  GHz was the worst of the four channels, with the radiosonde-calculated value less than the GVR measurement. The sense of this difference can also be seen on Fig. 5. This line is nearest to the spectroscopic “pivot point”, at which specifications in line width and intensity should compensate for each other (Payne et al., 2008); nevertheless both Payne et al. (2008) and Turner et al. (2009) indicate that the spectroscopic specification closer to the center line may require further refining, a result supported further here.

Lacking the means for further evaluation, we relied on an evenly-weighted best-fit to all four channels to provide an estimate of the above-cloud water vapor path. Almost all cases showed a good general correspondence between the four channel radiances and that corresponding to a best-fit WVP value, similar to Fig. 5. For above-cloud legs with little  $T_b$  variability, we estimate the error in the retrieved WVP at 0.2 mm; closer to the coast the  $T_b$  variability may not be fully represented in the retrieved WVPs.

### 3.4 Project-summary free-tropospheric WVPs

The distribution of the retrieved leg-mean free-tropospheric (above-cloud) water vapor paths are shown as a function of longitude for all fourteen research flights in Fig. 8a), and, for the near-coastal legs, as a function of latitude (Fig. 8b). The above-cloud flight legs were typically higher further off-shore. Free-tropospheric WVPs were often below 2 mm, and occasionally higher near the coast, particularly above the Arica Bight.

The highest WVP values in Fig. 8a were consistent with other information from their flights. Two of the WVP values approaching 1 cm came from the first and last above-cloud leg for the 23 October (RF4) flight, near Arica. Flight notes reported a haze and pollution layer at 3 km, with the aircraft sounding out of Arica showing relative humidities >30 % above 3 km. The other high free-tropospheric WVP value of 0.8 mm came from 2 November (RF8) from the first above-cloud leg, also near Arica, after the aircraft ascent had sampled a second moisture layer between 2–3 km, with RH ~30 %, above the boundary layer. Most of the higher-WVP points west of 75° came from the daytime flights.

Sounding-derived water vapor paths are also shown in Fig. 8 for VOCALS-REx (orange, 207 sondes) and the Oct-Nov cruises in 2001, 2003, 2006 and 2007 (purple, 293 sondes), calculated using the mean above-cloud aircraft altitude for each 2.5° bin. These show that the GVR- and sonde-derived values for 2008 were similar, despite different sampling days, with a drier free-troposphere in 2008 than in other years (consistent with Fig. 2 but using the GVR-derived dataset).

#### 4 Sub-cloud WVP and LWP retrieval methodology

The free-tropospheric WVPs were summed with boundary-layer WVPs computed from in-situ thermodynamic data gathered during the sub-cloud legs. The total WVP was then used as a separate input into a physical LWP retrieval modified from that of Zuidema et al. (2005). An estimate of the cloud temperature (to which the microwave absorption is sensitive) was made from the cloud boundaries and the sounding composites shown in Fig. 6 and included in the retrieval. Brightness temperatures were computed as a function of LWP, with the LWPs iterated upon until a best-fit to the measured  $\pm 14$  GHz  $T_b$  was found. Other approaches for deriving LWP from the GVR measurements include a neural net (Pazmany, 2006) and a four-channel physical retrieval (Cadeddu et al., 2007). The neural net algorithm had been developed from Barrow, Alaska sounding profiles not representative of subtropical stratocumulus, while

### Millimeter-wave stratocumulus LWP retrievals

P. Zuidema et al.

Title Page

Abstract

Introduction

Conclusions

References

Tables

Figures

◀

▶

◀

▶

Back

Close

Full Screen / Esc

Printer-friendly Version

Interactive Discussion



the four-channel retrieval is more applicable to lower-WVP environments. For the LWP retrieval in place here, both the boundary-layer WVPs and the LWPs retrieved for both the sub-cloud and cloud-base legs were done at 1 Hz temporal resolution.

The boundary layer water vapor path was calculated, at 1 Hz resolution, by integrating the in-situ water vapor mixing ratio from flight level up to either the lifting condensation level, or, to one-half of the altitude difference up to the cloud base. The mixing ratio at cloud base was used between this level and cloud base. This approach acknowledges some uncertainty in the calculation of the lifting condensation level (LCL). The cloud base temperature, needed to calculate the cloud base mixing ratio, was estimated from the larger of the aircraft infrared radiometer, or, that estimated using a dry adiabatic lapse rate. This was done to account for decoupling, wherein a dry adiabatic lapse rate would generate a too-low cloud base temperature, biasing the cloud base mixing ratio and ultimately the boundary layer WVP. Above cloud base, liquid water was adiabatically removed from the water vapor mixing ratio up to the radar-inferred cloud top. Cloud temperature was estimated at 100 m below cloud top from composite sondes constructed from the cruise radiosonde dataset at three off-shore distances: coastal, 300–600 km, and 600–1000 km (Fig. 6).

Data issues included cloud boundary determination, lidar availability, and the assumed moisture and temperature profiles. If cloud boundary information was missing when the measured GVR radiances suggested presence of cloud, the leg-mean cloud boundaries were used. If no radar cloud top was determined during the entire subcloud leg (more likely to occur than no cloud bases), the neighboring ascent and/or descent legs were used to estimate a leg-mean boundary-layer WVP. For the RF9 flight (9 November), the cloud lidar malfunctioned. The boundary-layer mean WVP was again estimated from the aircraft profile legs, but the accuracy of the RF9 GVR LWP retrievals was difficult to assess. Some of the research flights prior to RF9 encountered lidar timing problems, and these were corrected for as best as possible. Although the retrievals were generally insensitive to details of the radiosonde moisture and temperature profile, in a few near-coastal cases, the LWP iteration could not be made consistent with

## Millimeter-wave stratocumulus LWP retrievals

P. Zuidema et al.

Title Page

Abstract

Introduction

Conclusions

References

Tables

Figures

◀

▶

◀

▶

Back

Close

Full Screen / Esc

Printer-friendly Version

Interactive Discussion





## 5.1 Comparison to adiabatic LWPs

The accuracy of the adiabatically-derived LWPs also depended on how well the cloud boundaries are characterized. The cloud radar detected cloud top given sufficiently strong scatterers, at a vertical resolution of 30 m. The cloud lidar provided a sensitive detection of cloud base to within 3.75 m when precipitation was not present. A cloud thickness uncertainty of 30 m corresponded to a cloud liquid water path uncertainty of (30 %, 20 %, 15 %) for a (200, 300, 400) m thick cloud. Thus, thick yet non-drizzling clouds within well-mixed boundary layers were ideal for assessing the GVR LWPs with their adiabatically-derived counterparts.

Many sub-cloud legs took place in apparently well-mixed boundary layers, but most of these had mean LWPs closer to  $100 \text{ g m}^{-2}$  (for a mean cloud thickness closer to 300 m). Our best-case example, from the 21 October flight, had a mean cloud thickness of  $\sim 450$  m and a mean LWP slightly above  $200 \text{ g m}^{-2}$  (RF3SC2, Fig. 9), with the cloud base and LCL often closely aligned. The above-cloud WVP was 1.2 and 1.5 mm before and after this leg; values were linearly interpolated across the sub-cloud leg. The column-maximum radar reflectivity primarily fluctuated between  $-20$  and  $-10$  dBZ, and was typically below cloud top, suggesting a robust radar-inferred cloud top. The bordering aircraft ascents and descents indicated well-mixed conditions with minimal cloud-top entrainment.

The agreement between the GVR and adiabatically-derived LWP was excellent, with only a 2 % difference between their means (Fig. 9). This was true even towards the end of the leg, where the boundary layer would be considered decoupled by our CBH-LCL threshold. This reflected the radiative top-down mixing occurring within the cloud, whereby the cloud itself can remain well-mixed. The cloud base heights quickly adjusted to changes in the liquid water path, despite the sub-cloud thermodynamic discouragement of liquid water replenishment through moisture turbulent transport.

The RF3 flight sampled a particularly deep boundary layer with high LWPs and significant precipitation, yet conditions remained overcast. A statistical comparison between

### Millimeter-wave stratocumulus LWP retrievals

P. Zuidema et al.

Title Page

Abstract

Introduction

Conclusions

References

Tables

Figures

⏪

⏩

◀

▶

Back

Close

Full Screen / Esc

Printer-friendly Version

Interactive Discussion



the GVR and adiabatic LWP distributions from all nine subcloud legs of RF3 is shown in Fig. 10. The two distributions were basically identical for LWPs of 200 and 400  $\text{g m}^{-2}$ , lending further confidence to the GVR retrievals. The GVR LWP sample size was larger, however ( $N = 5471$  vs. an adiabatic sample size of 4003), because of the GVR's ability to retrieve LWPs for thinner clouds. For the two subcloud legs nearest the coast, GVR-retrieved LWPs were available and the lidar inferred complete cloud cover, but no radar determination of cloud top was made, and no adiabatic LWP estimates.

Summary statistics for three longitude bands are shown for the four nighttime flights that flew along 20° S out to 85° W and back on 21, 23 and 25 October, and 6 November (RF 3, 4, 5, and 10) in Fig. 11. These flights flew the pattern shown in Fig. 1, leaving Arica, Chile near midnight and returning at dawn. The larger frequency of occurrence of thinner clouds near the coast was clear: the GVR returned  $\sim$  three times as many samples as could be estimated adiabatically, and 45 % and 86 % of the GVR samples possessed LWPs  $< 40$  and  $100 \text{ g m}^{-2}$  respectively. Clouds with LWPs between 100 and 400  $\text{g m}^{-2}$  appeared to be consistently adiabatic, with little evidence of dilution at cloud top. This may be a particular physical feature of southeast Pacific stratocumulus, but may also be because the cloud radar could not sense highly-diluted regions near cloud top. Higher LWPs west of 80° W were consistent with deeper boundary layers and a greater propensity for precipitation (Zuidema et al., 2009; Leon et al., 2008) but even here the GVR retrieved 1.5 times as many LWPs as were adiabatically estimated, with 23 % and 50 % of the GVR LWPs being  $< 40$  and  $100 \text{ g m}^{-2}$ .

The correspondence between GVR and the adiabatic LWPs for LWPs  $> 400 \text{ g m}^{-2}$  was poorer than for LWPs  $< 400 \text{ g m}^{-2}$  in Figs. 9 and 10. Several causes in combination likely contributed. For higher LWPs precipitation-induced sub-cloud decoupling was likely, possibly reducing the near-cloud-base water vapor mixing ratio below the value used to estimate the boundary-layer WVP. The retrieved LWP would then be underestimated. The measured millimeter-wave  $T_b$ s may also be influenced by both Mie attenuation and scattering from the larger drop sizes, effects that in turn would under- and over-estimate the true LWP. In addition, the lidar-determined cloud base may be

## Millimeter-wave stratocumulus LWP retrievals

P. Zuidema et al.

Title Page

Abstract

Introduction

Conclusions

References

Tables

Figures

◀

▶

◀

▶

Back

Close

Full Screen / Esc

Printer-friendly Version

Interactive Discussion



placed lower than the active cloud layer either because of the precipitation, or because of a lower, inactive, scud cloud layer.

For thin clouds, which mostly occurred near the coast, other uncertainties may be embedded in the LWP retrievals. Large variations in free-tropospheric water vapor path during a sub-cloud leg may have been an issue. Thin clouds generally had lower radar reflectivities, and a cloud top height was less likely to be reported, affecting the boundary layer water vapor specification.

## 5.2 Clear-sky LWPs, and cloudy skies without liquid

The four 20° S flights highlighted in Fig. 11 experienced a mean cloud cover of 94 %, with few clear-sky LWPs. We increased the statistics available for an error analysis by evaluating the clear-sky and cloud-base-only conditions of the subcloud legs of thirteen research flights (RF9 was excluded). These totaled 60 590 1 Hz samples, equivalent to 7270 km at an average flight speed of 120 m s<sup>-1</sup>. Skies were cloudy 90 % of the time according to either the ceilometer or cloud radar (precipitation at times obfuscated the cloud base), but non-zero LWPs were retrieved only 63 % of the time.

Figure 12a shows the distribution of LWPs retrieved during the 8.6 % of the time determined to be clear (i.e., neither the lidar nor the radar returned a signal). Several legs were excluded from this statistic, because they sampled open cellular convection with obviously irregular lidar and radar returns (e.g., RF13SC3) or, more rarely, the input moisture and temperature profiles could not be manipulated to adequately represent a highly decoupled boundary layer (e.g., RF13pocsc2b). Clear skies, within this data sample, possessed a LWP cloud fraction of 3 %, with 80 % of those retrieved LWPs < 20 g m<sup>-2</sup>. In other words, the GVR was unlikely to perform a LWP retrieval in skies deemed clear by the lidar.

In cases where the lidar did sense a cloud base but the radar did not determine a cloud top, the GVR-retrieved LWPs also depended on if the conditions were coupled or decoupled. Coupled and decoupled conditions constituted 11 % and 12.5 % of the cases with an established cloud base, respectively ( $N = 6179$  and 7100). In decoupled

### Millimeter-wave stratocumulus LWP retrievals

P. Zuidema et al.

Title Page

Abstract

Introduction

Conclusions

References

Tables

Figures

◀

▶

◀

▶

Back

Close

Full Screen / Esc

Printer-friendly Version

Interactive Discussion



conditions, the GVR retrieval was much more likely to miss the cloud entirely than in coupled conditions: 74 % versus 59 %. The distributions of the LWPs, when they were retrieved, are shown in Fig. 12b and c. The LWPs retrieved within decoupled conditions were generally lower than in coupled conditions. While physically plausible because upward moisture transport was discouraged by the decoupling, the result may also be a retrieval artifact, in that the input water vapor path is more likely to be over-estimated in decoupled conditions. This will decrease the retrieved LWP, and increase the likelihood that a LWP is not retrieved at all. Further work can be done to improve the LWP retrievals in decoupled conditions by using all four channels and implementing a physical retrieval similar to that of Cadeddu et al. (2007), if the WVPs are low.

## 6 Statistical summary

The distribution of retrieved and adiabatic LWPs from the subcloud legs for all research flights except RF9 is shown in Fig. 13, subdivided by coupling. 52 % of all the samples were classified as decoupled (Table 1). The retrieved LWP cloud fraction was 71 % for the well-coupled boundary layers, versus 67 % for the decoupled boundary layers. Of the retrieved values, 65 % and 61 % of the LWPs were  $<100 \text{ g m}^{-2}$  for the coupled and decoupled samples, respectively. The adiabatic LWP cloud fraction, in contrast, was higher for the decoupled cases (51 %) than for the well-mixed cases (42 %). This was explained by the greater frequency of radar cloud top returns for the decoupled cases, as many of the decoupled samples came from the flights that sampled open cellular convection, and thereby had higher reflectivities from precipitation and larger drop sizes (Fig. 13c) than did the well-mixed cases. The distributions of the GVR and adiabatic LWPs under decoupled conditions were also more similar than under coupled conditions: local precipitation, leading to intermittent decoupling within an otherwise well-coupled boundary layer (see, e.g., Fig. 9) could be consistent with both well-determined adiabatic and GVR LWPs. Overall, liquid water paths greater than  $\sim 160 \text{ g m}^{-2}$  were determined well by both adiabatic and millimeter-wave approaches

### Millimeter-wave stratocumulus LWP retrievals

P. Zuidema et al.

Title Page

Abstract

Introduction

Conclusions

References

Tables

Figures



Back

Close

Full Screen / Esc

Printer-friendly Version

Interactive Discussion



under both coupled and decoupled conditions, and the biggest difference between the coupled and decoupled cases was in the detection of thin clouds.

## 7 Conclusions

Brightness temperatures from a millimeter-wave radiometer on board the NCAR C-130 plane were used to retrieve above-cloud water vapor paths, and, were combined with in-situ thermodynamic data to retrieve liquid water paths during the sub-cloud legs. The retrieved above-cloud water vapor paths were on par with surface-based Arctic values, indicating a broad infrared spectrum was available for radiative cooling of the cloud top. A comparison of the VOCALS retrieved free-tropospheric WVPs to radiosonde-derived values from previous years suggests that the free-troposphere sampled during VOCALS was drier than in other years, with values ranging from one to two mm offshore to almost one cm near the coast.

The leg-mean LWP error in well-coupled conditions can originate from incorrect specification of the above-cloud WVP (estimated at 0.2 mm, or 6–10 g m<sup>-2</sup>), and a 2 K absolute and 0.5 K relative uncertainty in the GVR  $T_b$ , corresponding to 10–20 g m<sup>-2</sup> and 2–5 g m<sup>-2</sup>, respectively. Based on these number we conservatively estimate the absolute leg-mean LWP uncertainty to be ~25 g m<sup>-2</sup> and the relative (within-leg) uncertainty at <10 g m<sup>-2</sup>. The uncertainties will be higher in heavily-precipitating conditions. Further work may be done to assess LWPs in decoupled conditions, particularly for the pockets of open cells for which the thin cloud layer identified at the top of the open cells (e.g., Wood et al., 2011a) is of interest. Radiosonde profiles could be assessed more systematically, or, all four GVR channels could be invoked to simultaneously retrieve the WVP and LWP if the above-aircraft WVP does not saturate the center absorption lines.

The GVR-retrieved LWPs compared well against adiabatically-derived LWPs between 200–400 g m<sup>-2</sup> in best-case comparisons. The GVR-retrieved LWPs provided further support for a view of the southeast Pacific stratocumulus as close to its adiabatic

### Millimeter-wave stratocumulus LWP retrievals

P. Zuidema et al.

Title Page

Abstract

Introduction

Conclusions

References

Tables

Figures

◀

▶

◀

▶

Back

Close

Full Screen / Esc

Printer-friendly Version

Interactive Discussion



**Millimeter-wave  
stratocumulus LWP  
retrievals**

P. Zuidema et al.

Title Page

Abstract

Introduction

Conclusions

References

Tables

Figures

◀

▶

◀

▶

Back

Close

Full Screen / Esc

Printer-friendly Version

Interactive Discussion



LWP maximum, with little cloud-top dilution offshore, but a decrease in radar sensitivity to the diluted cloud tops may exaggerate this perception. A particular strength of the higher  $183 \pm 14$  GHz frequency was the ability to retrieve liquid water paths for thin clouds. Clouds with LWPs  $< 100 \text{ g m}^{-2}$  composed almost two-thirds of the entire dataset. These were more frequent near the coast, near continental aerosol sources. The GVR dataset may prove to be particularly useful for aerosol susceptibility studies.

For VOCALS-REx a cloud radar (zenith and nadir viewing) and cloud lidar (zenith-viewing) were also a part of the C-130 plane research instrumentation: the 94 GHz (3.2 mm wavelength) Wyoming cloud radar, and the Wyoming cloud lidar (Wang et al., 2009) operating at a 355 nm wavelength. The three cloud remote sensors provided complementary cloud metrics that have been combined into Integrated Datasets. These are publicly available for each research flight through the VOCALS EOL data archive. The combined datasets free users from obtaining data for the individual instruments and from some of the data processing, extending possibilities for process studies of stratocumulus over the remote ocean (see, e.g., Wood et al., 2011a).

While the VOCALS experiment was the first – and last – field deployment on the C-130 of the airborne GVR, the airborne GVR has features that recommend further aircraft deployments of similar instrumentation. It is small and easily integrated onto an aircraft platform, inexpensive, and its zenith-pointing orientation eases the LWP retrievals and allows for concurrent sub-cloud air sampling. The millimeter-wavelengths were not optimal for the subtropical stratocumulus region because the center lines saturated, but data from such an instrument could be combined with that from an instrument with a frequency channel focused on establishing the water vapor path, such as around the 22 GHz water vapor absorption line.

*Acknowledgements.* PZ acknowledges support from the NSF Large-Scale Dynamics Division under Award 0745470.

## References

- Bennartz, R., Lauer, A., and Brenguier, J.-L.: Scale-aware integral constraints on autoconversion and accretion in regional and global climate models, *Geophys. Res. Lett.*, 38, L10809, doi:10.1029/2011GL047618, 2011. 19582
- 5 Bretherton, C. S., Wood, R., George, R. C., Leon, D., Allen, G., and Zheng, X.: Southeast Pacific stratocumulus clouds, precipitation and boundary layer structure sampled along 20° S during VOCALS-REx, *Atmos. Chem. Phys.*, 10, 10639–10654, doi:10.5194/acp-10-10639-2010, 2010. 19592
- 10 Cadeddu, M. P. and Turner, D. D.: Evaluation of water permittivity models from ground-based observations of cold clouds at frequencies between 23 and 170 GHz, *IEEE T. Geosci. Remote Sens.*, in press, 2011. 19587
- Cadeddu, M. P., Liljegren, J. C., and Pazmany, A. L.: Measurements and retrievals from a new 183-GHz water vapor radiometer in the Arctic, *IEEE T. Geosci. Remote Sens.*, 45, 2207–2215, 2007. 19584, 19586, 19587, 19588, 19590, 19596
- 15 Cahalan, R. F., Ridgway, W., Wiscombe, W. J., Gollmer, S., and Harshvardhan: Independent Pixel and Monte Carlo Estimates of Stratocumulus Albedo, *J. Atmos. Sci.*, 51, 3776–3790, 1994. 19582
- Cimini, D., Westwater, E. R., Gasiewski, A., Klein, M., Leuski, V. Y., and Liljegren, J.: Ground-based millimeter- and submillimeter-wave observations of low vapor and liquid water contents, *IEEE T. Geosci. Remote Sens.*, 45, 2169–2180, 2007. 19584
- 20 Cimini, D., Nasir, F., Westwater, E. R., Payne, V. H., Turner, D. D., Mlawer, E. J., Exner, M. L., and Cadeddu, M. P.: Comparison of ground-based millimeter-wave observations and simulations in the Arctic winter, *IEEE T. Geosci. Remote Sens.*, 47, 3098–3106, 2009. 19584, 19586
- 25 de Szoeko, S., Fairall, C. W., Wolfe, D., Bariteau, L., and Zuidema, P.: Surface flux observations on the Southeastern tropical Pacific Ocean and attribution of SST errors in coupled ocean-atmosphere models, *J. Climate*, 23, 4152–4174, 2010. 19584
- Hewison, T.: Aircraft validation of clear air absorption models at millimeter wavelengths (89–183 GHz), *J. Geophys. Res.*, 111, D14303, doi:10.1029/2005JD006719, 2006. 19587
- 30 Jones, C. R., Bretherton, C. S., and Leon, D.: Coupled vs. decoupled boundary layers in VOCALS-REx, *Atmos. Chem. Phys. Discuss.*, 11, 8431–8460, doi:10.5194/acpd-11-8431-2011, 2011. 19592

### Millimeter-wave stratocumulus LWP retrievals

P. Zuidema et al.

Title Page

Abstract

Introduction

Conclusions

References

Tables

Figures



Back

Close

Full Screen / Esc

Printer-friendly Version

Interactive Discussion



## Millimeter-wave stratocumulus LWP retrievals

P. Zuidema et al.

Title Page

Abstract

Introduction

Conclusions

References

Tables

Figures

◀

▶

◀

▶

Back

Close

Full Screen / Esc

Printer-friendly Version

Interactive Discussion



Leon, D., Wang, Z., and Liu, D.: Climatology of drizzle in marine boundary layer clouds based on one year of data from CloudSat and CALIPSO, *J. Geophys. Res.*, 113, D00A14, doi:10.1029/2008JD009835, 2008. 19594

Liebe, H. J., Hufford, G. A., and Manabe, T.: A model for the complex permittivity of water at frequencies below 1 THz, *Int. J. Infrared Millimeter Waves*, 12, 659–675, 1991. 19587

Liebe, H. J., Hufford, G. A., and Cotton, M. G.: Propagation modeling of moist air and suspended water/ice particles at frequencies below 1000 GHz, *Atmospheric Propagation Effects through Natural and Man-Made Obscurants for Visible through MM-wave radiation*, aGARD-CP-542, 3.1–3.10, 1993. 19587

Liljegren, J. C., Boukabara, S. A., Cady-Pereira, K., and Clough, S. A.: The effect of the half-width of the 22-GHz water vapor line on retrievals of temperature and water vapor profiles with a twelve-channel microwave radiometer, *IEEE T. Geosci. Remote Sens.*, 43, 1102–1108, 2005. 19587

Liu, G., Shao, H., Coakley, J. A., Curry, J. A., Haggerty, J. A., and Tschudi, M. A.: Retrieval of cloud droplet size from visible and microwave radiometric measurements during INDOEX: Implication to aerosols' indirect radiative effect, *J. Geophys. Res.*, 108, 4006, doi:10.1029/2001JD001395, 2003. 19582, 19583

McComiskey, A., Feingold, G., Frisch, S., Min, Q., Turner, D., and Miller, M.: An assessment of aerosol-cloud interactions in marine stratus clouds based on surface remote sensing, *J. Geophys. Res.*, 114, D09203, doi:10.1029/2008JD011006, 2009. 19583

Miloshevich, L. M., Vomel, H., Whiteman, D., Lesht, B., Schmidlin, F., and Russo, F.: Absolute accuracy of water vapor measurements from six operational radiosonde types launched during AWEX-G and implications for AIRS validation, *J. Geophys. Res.*, 111, D09S10, doi:10.1029/2005JD006083, 2006. 19584, 19589

Miloshevich, L. M., Vomel, H., Whiteman, D., and Leblanc, T.: Accuracy assessment and correction of Vaisala RS92 radiosonde water vapor measurements, *J. Geophys. Res.*, 114, D11305, doi:10.1029/2008JD011565, 2009. 19584, 19588

O'Dell, C. W., Wentz, F. J., and Bennartz, R.: Cloud liquid water path from satellite-based passive microwave observations: a new climatology over the global oceans, *J. Climate*, 21, 1721–1739, 2008. 19582

Payne, V. H., Delamere, J. S., Cady-Pereira, K. E., Gamache, R., Moncet, J.-L., Mlawer, E. J., and Clough, S. A.: Air-broadened half-widths of the 22- and 183-GHz water-vapor lines, *IEEE T. Geosci. Remote Sens.*, 46, 3601–3617, 2008. 19584, 19587, 19588, 19589

## Millimeter-wave stratocumulus LWP retrievals

P. Zuidema et al.

Title Page

Abstract

Introduction

Conclusions

References

Tables

Figures

◀

▶

◀

▶

Back

Close

Full Screen / Esc

Printer-friendly Version

Interactive Discussion



Pazmany, A.: A compact 183 GHz radiometer for airborne and ground-based water vapor and liquid water sensing, *IEEE Trans. Geosci. Remote Sens.*, 45, 2202–2206, 2006. 19583, 19584, 19585, 19586, 19590

Racette, P., Westwater, E., Han, Y., Gasiewski, A., Klein, M., Cimini, D., Jones, D., Manning, W., Kim, E., Wang, J., Leuski, V., and Kiedron, P.: Measurement of low amounts of precipitable water vapor using ground-based millimeterwave radiometry, *J. Atmos. Ocean. Tech.*, 22, 317–337, 2005. 19584, 19588

Rosenkranz, P. W.: Water vapor microwave continuum absorption: A comparison of measurements and models, *Radio Sci.*, 33, 919–928, 1998. 19587

Seethala, C. and Horvath, A.: Global assessment of AMSR-E and MODIS cloud liquid water path retrievals in warm oceanic clouds, *J. Geophys. Res.*, 115, D13202, doi:10.1029/2009JD012662, 2010. 19582

Siebesma, A. P., Jakob, C., Lenderink, G., Neggers, R. A., Teixeira, J., Meijgaard, E. V., Calvo, J., Chlond, A., Grenier, H., Jones, C., Kohler, M., Kitagawa, H., Marquet, P., Lock, A. P., Muller, F., Olmeda, D., and Severijns, C.: Cloud representation in General Circulation Models over the Northern Pacific Ocean: A EUROCS intercomparison study, *Q. J. Roy. Meteorol. Soc.*, 130, 3245–3267, 2004. 19582

Turner, D. D. and Mlawer, E. J.: The radiative heating in underexplored bands campaigns, *B. Am. Meteor. Soc.*, 91, 911–923, 2010. 19584

Turner, D. D., Cadetdu, M. P., Lohnert, U., Crewell, S., and Vogelmann, A. M.: Modifications to the water vapor continuum in the microwave suggested by ground-based 150-GHz observations, *IEEE T. Geosci. Remote Sens.*, 47, 3326–3337, 2009. 19587, 19589

Wang, Z., Wechsler, P., Kuestner, W., French, J., Rodi, A., Glover, B., Burkhart, M., and Lukens, D.: Wyoming Cloud Lidar: instrument description and applications, *Opt. Ex.*, 17(16), 13576–13587, 2009. 19598

Wood, R., Bretherton, C., and Hartmann, D. L.: Diurnal cycle of liquid water path over the subtropical and tropical oceans, *Geophys. Res. Lett.*, 29, 2092, doi:10.1029/2002GL015371, 2002. 19582

Wood, R., Kohler, M., Bennartz, R., and O'Dell, C.: The diurnal cycle of surface divergence over the global oceans, *Q. J. Roy. Meteor. Soc.*, 135, 1484–1493, 2009. 19582

Wood, R., Bretherton, C. S., Leon, D., Clarke, A. D., Zuidema, P., Allen, G., and Coe, H.: An aircraft case study of the spatial transition from closed to open mesoscale cellular convection over the Southeast Pacific, *Atmos. Chem. Phys.*, 11, 2341–2370, doi:10.5194/acp-11-2341-

## Millimeter-wave stratocumulus LWP retrievals

P. Zuidema et al.

Title Page

Abstract

Introduction

Conclusions

References

Tables

Figures

⏪

⏩

◀

▶

Back

Close

Full Screen / Esc

Printer-friendly Version

Interactive Discussion



2011, 2011a. 19597, 19598

Wood, R., Mechoso, C. R., Bretherton, C. S., Weller, R. A., Huebert, B., Straneo, F., Albrecht, B. A., Coe, H., Allen, G., Vaughan, G., Daum, P., Fairall, C., Chand, D., Gallardo Klenner, L., Garreaud, R., Grados, C., Covert, D. S., Bates, T. S., Krejci, R., Russell, L. M., de Szoeko, S.,  
5 Brewer, A., Yuter, S. E., Springston, S. R., Chaigneau, A., Toniazzo, T., Minnis, P., Palikonda, R., Abel, S. J., Brown, W. O. J., Williams, S., Fochesatto, J., Brioude, J., and Bower, K. N.: The VAMOS Ocean-Cloud-Atmosphere-Land Study Regional Experiment (VOCALS-REx): goals, platforms, and field operations, *Atmos. Chem. Phys.*, 11, 627–654, doi:10.5194/acp-11-627-2011, 2011b. 19583

10 Zhu, P., Bretherton, C., Koehler, M., Cheng, A., Chlond, A., Geng, Q., Austin, P., Golaz, J.-C., Lenderink, G., Lock, A., and Stevens, B.: Intercomparison and Interpretation of Single-Column Model Simulations of a Nocturnal Stratocumulus-topped Marine Boundary Layer, *Mon. Weather Rev.*, 133, 2741–2758, 2005. 19582

15 Zuidema, P., Westwater, E. R., Fairall, C., and Hazen, D.: Ship-based liquid water path estimates in marine stratocumulus, *J. Geophys. Res.*, 110, D20206, doi:10.1029/2005JD005833, 2005. 19582, 19587, 19590

Zuidema, P., Painemal, D., deSzoeko, S., and Fairall, C.: Stratocumulus cloud top height estimates and their climatic implications, *J. Climate*, 22, 4652–4666, 2009. 19584, 19594

## Millimeter-wave stratocumulus LWP retrievals

P. Zuidema et al.

Title Page

Abstract

Introduction

Conclusions

References

Tables

Figures

⏪

⏩

◀

▶

Back

Close

Full Screen / Esc

Printer-friendly Version

Interactive Discussion



**Table 1.** Number of 1 Hz samples contributing to the distributions shown in Fig. 13.

	$N$	$N_{\text{lwp}}$	$N_{\text{adlwp}}$
coupled	24 994	17 817	10 401
decoupled	26 842	18 048	13 791

## Millimeter-wave stratocumulus LWP retrievals

P. Zuidema et al.

Title Page

Abstract

Introduction

Conclusions

References

Tables

Figures

◀

▶

◀

▶

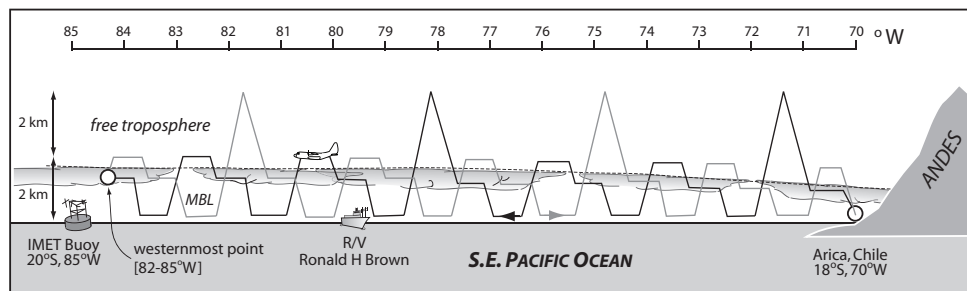
Back

Close

Full Screen / Esc

Printer-friendly Version

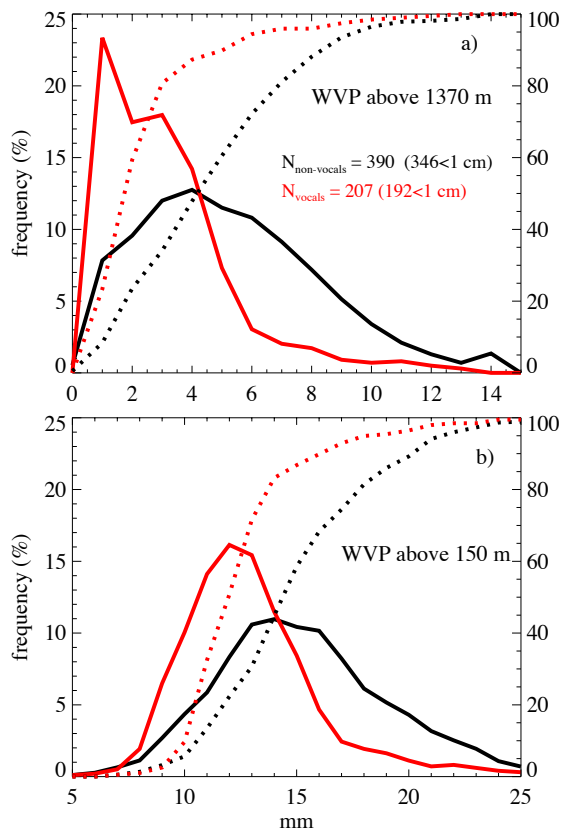
Interactive Discussion



**Fig. 1.** The NCAR C-130 flight plan along  $20^{\circ}$  S, with the outward leg in black and return leg in grey. Figure provided by Robert Wood.

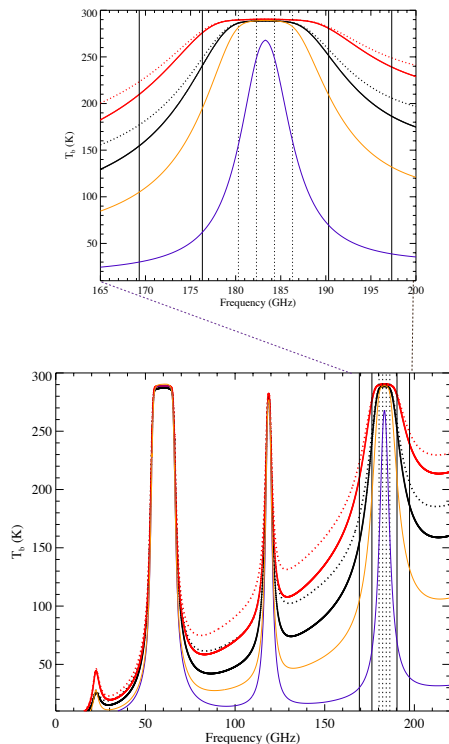
## Millimeter-wave stratocumulus LWP retrievals

P. Zuidema et al.



**Fig. 2.** (a) Percentage of occurrence of free-tropospheric water vapor path values calculated from ship-board Vaisala radiosondes excluding VOCALS, and VOCALS radiosondes (red line). Dashed lines indicate the cumulative frequency of occurrence. (b) Same as (a) but for the water vapor paths overlying the sub-cloud aircraft legs at 150 m altitude. All radiosondes were released between 0° and 23° S, east of 97° W and reached at least 200 hPa.

[Title Page](#)
[Abstract](#)
[Introduction](#)
[Conclusions](#)
[References](#)
[Tables](#)
[Figures](#)
[◀](#)
[▶](#)
[◀](#)
[▶](#)
[Back](#)
[Close](#)
[Full Screen / Esc](#)
[Printer-friendly Version](#)
[Interactive Discussion](#)

**Fig. 3.** Downwelling brightness temperatures ( $T_b$ ) at 150 m altitude calculated using the 10th and 90th percentile of the 330 RS-92 radiosondes reaching 50 hPa (WVPs of 1.1 and 2.1 cm, black and red lines respectively), for 0–220 GHz (bottom panel) and 165–200 GHz (top panel). Cloudy-sky (LWP =  $100 \text{ g m}^{-2}$ , cloud base at 1 km) spectra shown as dashed lines. Above-cloud spectra at 1370 m are also shown (WVPs of 1.86 and 9.8 mm, purple and yellow lines, respectively). Thin vertical lines indicate GVR frequencies, note these are combined into four double-sideband values within the radiometer.

## Millimeter-wave stratocumulus LWP retrievals

P. Zuidema et al.

Title Page

Abstract

Introduction

Conclusions

References

Tables

Figures



Back

Close

Full Screen / Esc

Printer-friendly Version

Interactive Discussion



## Millimeter-wave stratocumulus LWP retrievals

P. Zuidema et al.

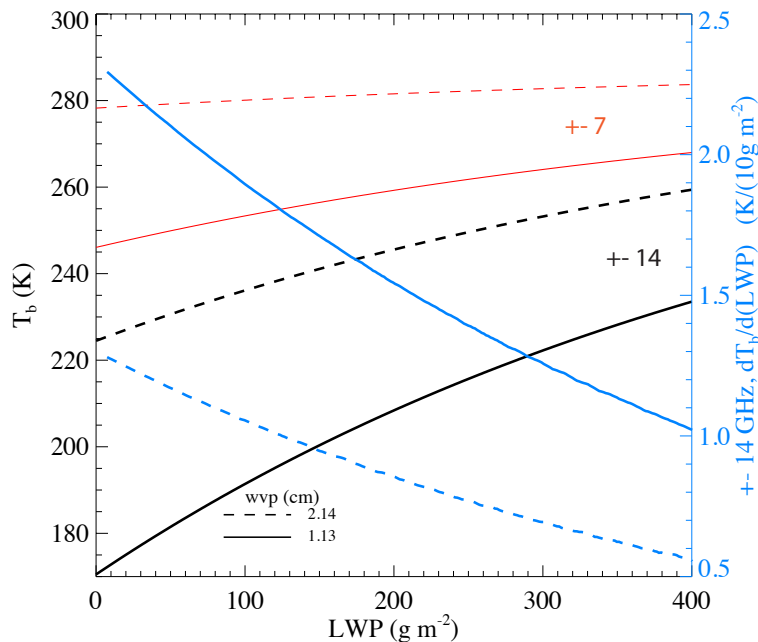


**Fig. 4.** Brightness temperatures for the outer wing channels ( $\pm 14$  and  $\pm 7$  GHz; black and red lines respectively) as a function of liquid water path at 150 m altitude for the 10th and 90th percentile (dashed and solid lines) water vapor profiles represented in Fig. 3. Brightness temperature sensitivity to LWP for the  $\pm 14$  GHz channel is shown in blue, values (decreasing to the right) are indicated by right-hand axis.

Title Page

Abstract

Introduction

Conclusions

References

Tables

Figures

◀

▶

◀

▶

Back

Close

Full Screen / Esc

Printer-friendly Version

Interactive Discussion



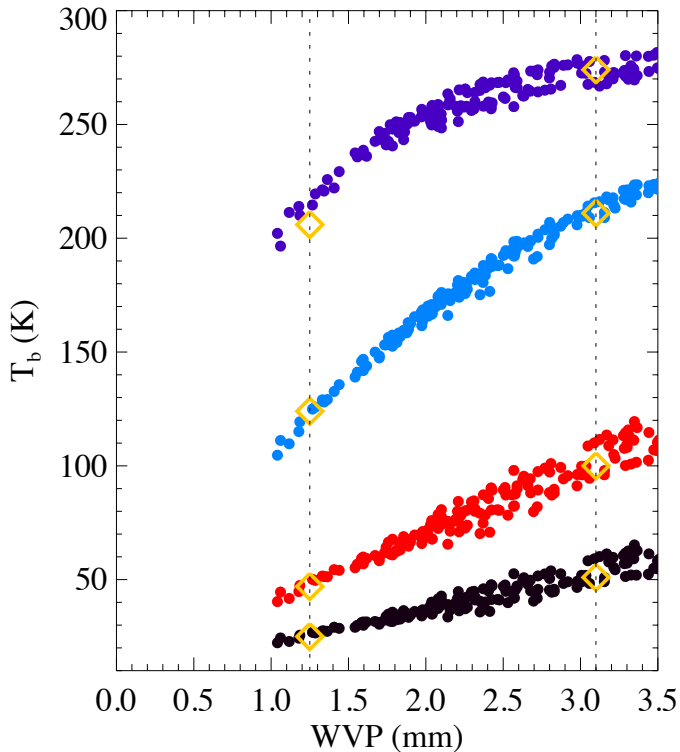


**Fig. 5.** Simulated  $T_b$  for the  $\pm 1$ ,  $\pm 3$ ,  $\pm 7$ , and  $\pm 14$  GHz GVR channels calculated for 330 RS92 soundings reaching 50 hPa (purple, blue, red, and black filled circles, respectively), and GVR 5-minute mean measurements from an example near-coastal above-cloud leg (RF3, AC1; yellow diamonds). Climatological stratospheric water vapor profiles were extrapolated beyond 50 hPa.

**Millimeter-wave  
stratocumulus LWP  
retrievals**

P. Zuidema et al.

Title Page

Abstract

Introduction

Conclusions

References

Tables

Figures

◀

▶

◀

▶

Back

Close

Full Screen / Esc

Printer-friendly Version

Interactive Discussion



**Millimeter-wave  
stratocumulus LWP  
retrievals**

P. Zuidema et al.

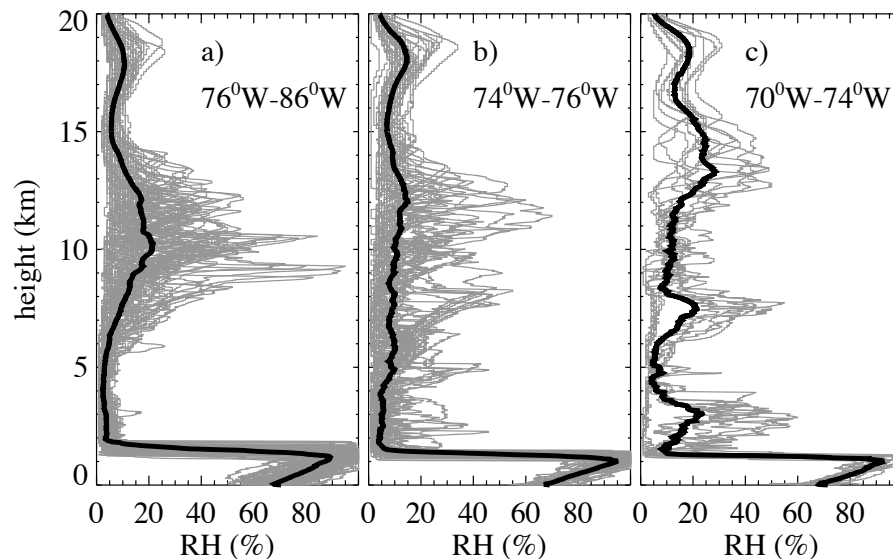


**Fig. 6.** Ship-launched soundings during VOCALS-REx along  $20^{\circ}$  S between (a)  $76^{\circ}$ – $86^{\circ}$  W ( $N = 77$ ), (b)  $74^{\circ}$ – $76^{\circ}$  W ( $N = 50$ ), and (c)  $70^{\circ}$ – $74^{\circ}$  W ( $N = 11$ ). Black lines indicate mean soundings for each longitude bin.

Title Page

Abstract

Introduction

Conclusions

References

Tables

Figures

◀

▶

◀

▶

Back

Close

Full Screen / Esc

Printer-friendly Version

Interactive Discussion



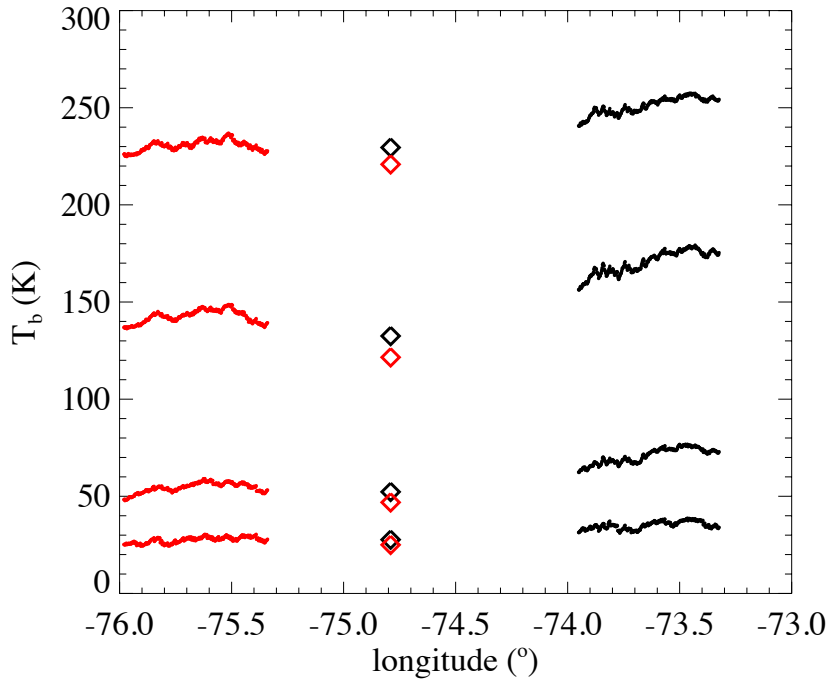


**Fig. 7.** Two above-cloud overpasses made during the 2 November nighttime flight (RF8 AC2 and AC4, occurring at 07:04:20 and 08:03:20 UTC, and 1.38 and 1.6 km altitude respectively; black and red time series traces). The  $T_b$ s simulated from a ship-launched radiosonde at 07:22:20 UTC at these altitudes are shown as black and red diamonds respectively.

**Millimeter-wave  
stratocumulus LWP  
retrievals**

P. Zuidema et al.

Title Page

Abstract

Introduction

Conclusions

References

Tables

Figures

◀

▶

◀

▶

Back

Close

Full Screen / Esc

Printer-friendly Version

Interactive Discussion



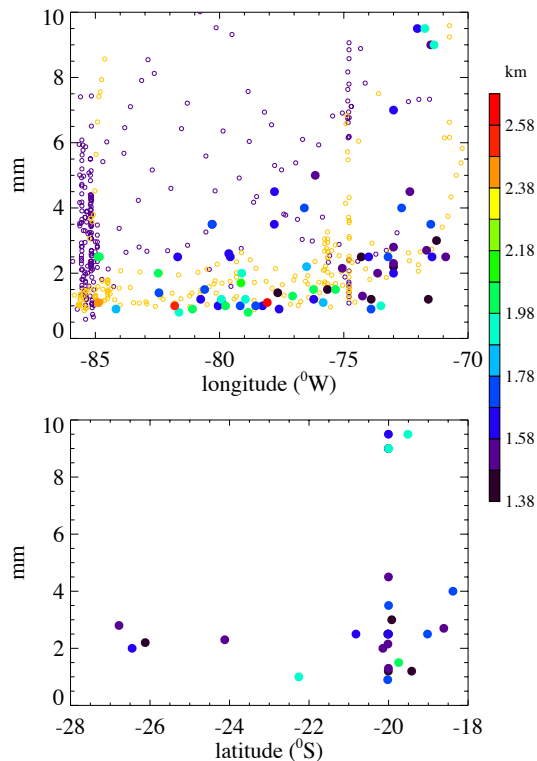


**Fig. 8.** Free-tropospheric water vapor paths retrieved from the above-cloud legs **(a)** of all research flights, as a function of longitude (85 legs), and **(b)** as a function of latitude for longitudes east of 75.5° W (42 legs). Colors indicate the leg altitude. Mean flight altitudes, when binned by 2.5° in longitude from 70° W westward, were, in meters, with the number of samples in parentheses: 1495 (14), 1370 (26), 1715 (10), 1695 (19), 1735 (11), and 1855 (5). These altitudes were used to calculate free-tropospheric WVP values from soundings launched from ship during VOCALS (orange,  $N = 207$ ) and cruises during 2001, 2003, 2006 and 2007 (purple,  $N = 293$ ).

**Millimeter-wave stratocumulus LWP retrievals**

P. Zuidema et al.

Title Page

Abstract

Introduction

Conclusions

References

Tables

Figures

◀

▶

◀

▶

Back

Close

Full Screen / Esc

Printer-friendly Version

Interactive Discussion



Millimeter-wave  
stratocumulus LWP  
retrievals

P. Zuidema et al.

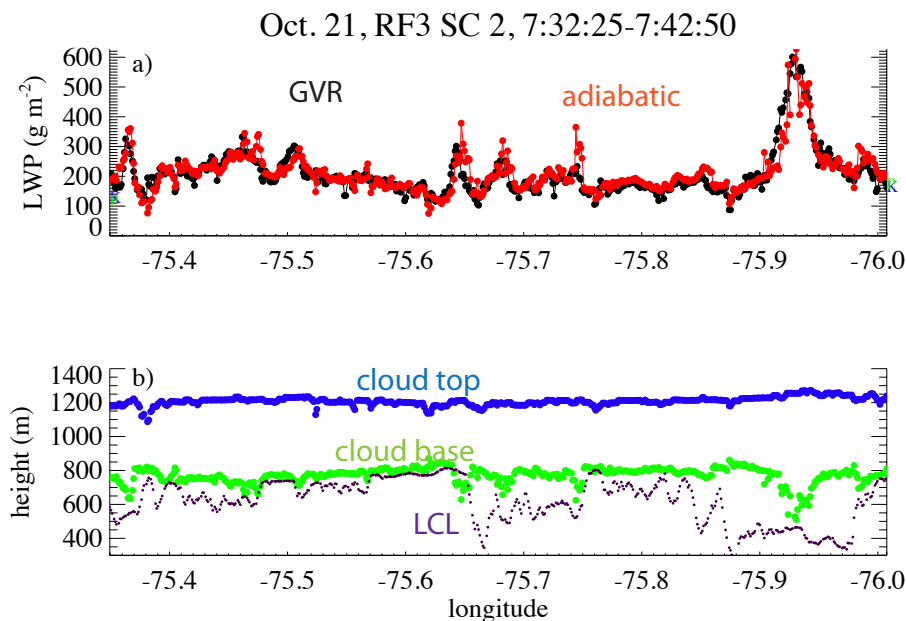


**Fig. 9.** (a) GVR-retrieved and adiabatically-derived LWP (black and red filled circles respectively) for RF3 SC2 leg (21 October, 02:32:25–02:42:50 LT). Retrieved and adiabatic LWP means (standard deviations) are 207 (76) and 211 (69)  $\text{g m}^{-2}$  respectively. Pre-descent and post-ascent LWP values derived from the FSSP and King probes are indicated as green and blue filled circles at beginning and end of the time series. (b) Corresponding lidar-inferred cloud base (green), the lifting condensation level (purple), and radar-derived cloud top (blue).

[Title Page](#)[Abstract](#)[Introduction](#)[Conclusions](#)[References](#)[Tables](#)[Figures](#)[◀](#)[▶](#)[◀](#)[▶](#)[Back](#)[Close](#)[Full Screen / Esc](#)[Printer-friendly Version](#)[Interactive Discussion](#)

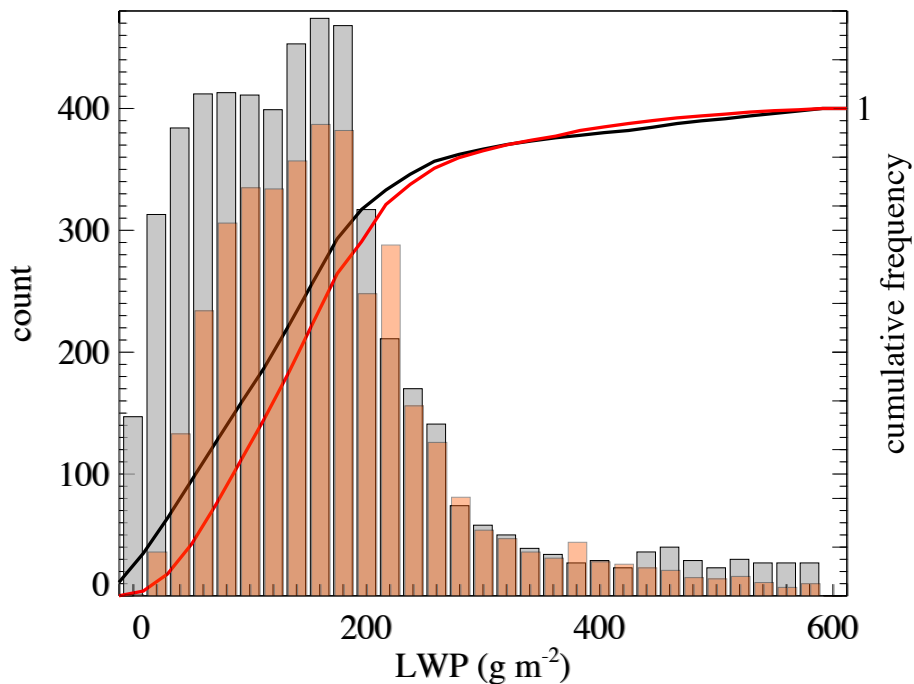


**Fig. 10.** Distribution of GVR-retrieved (black) and adiabatic (red) LWPs from all nine subcloud legs of the 21 October research flight (RF3). Total number of samples is 5471 and 4003 for the GVR and adiabatic calculation respectively. LWP bins of  $20 \text{ g m}^{-2}$ .

**Millimeter-wave stratocumulus LWP retrievals**

P. Zuidema et al.

Title Page

Abstract Introduction

Conclusions References

Tables Figures

◀ ▶

◀ ▶

Back Close

Full Screen / Esc

Printer-friendly Version

Interactive Discussion



## Millimeter-wave stratocumulus LWP retrievals

P. Zuidema et al.

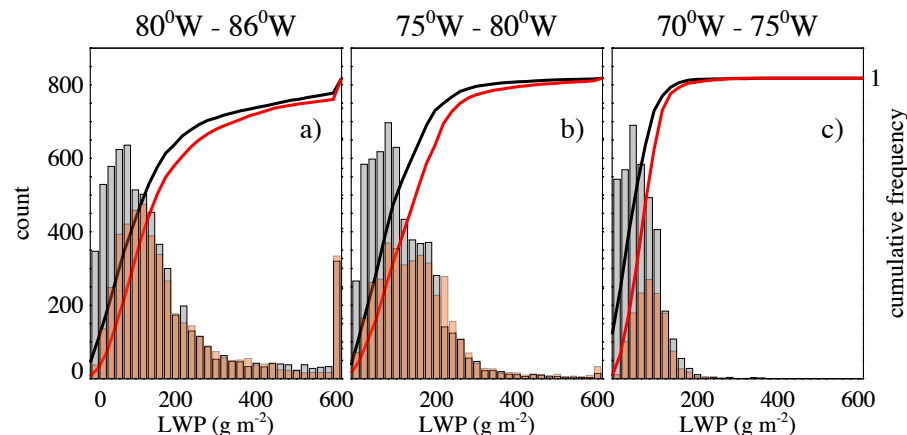


**Fig. 11.** Distributions of GVR-retrieved (black) and adiabatic (red) LWPs from the four research flights dedicated to a 20° S nighttime flight pattern out to 85° W (21, 23, 25 October and 6 November; RF 3, 4, 5 and 10) subdivided by longitude; **(a)** 80° W–86° W, **(b)** 75° W–80° W, and **(c)** 70° W–75° W. LWP bins of 20 g m<sup>-2</sup>. The cumulative frequencies for both the GVR-retrieved (black) and adiabatic (red) LWPs correspond to the right y-axis.

Title Page

Abstract

Introduction

Conclusions

References

Tables

Figures

◀

▶

◀

▶

Back

Close

Full Screen / Esc

Printer-friendly Version

Interactive Discussion



**Millimeter-wave  
stratocumulus LWP  
retrievals**

P. Zuidema et al.

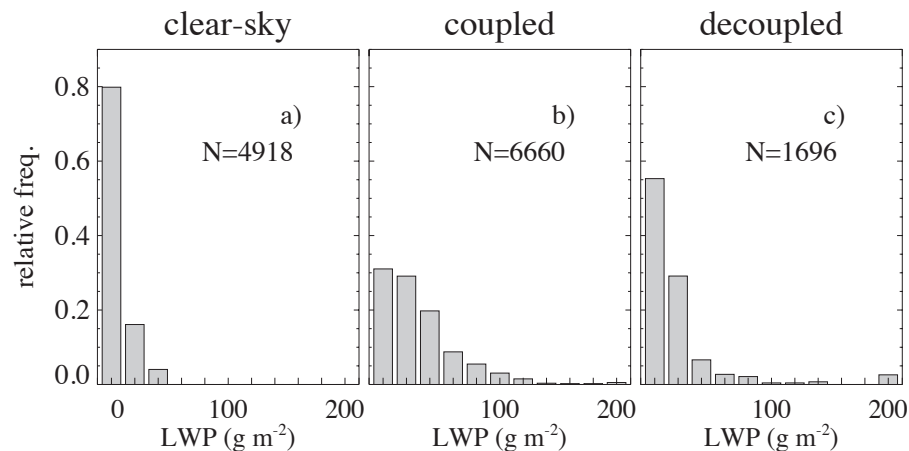


**Fig. 12.** Frequency distributions of the **(a)** clear-sky LWPs (i.e., neither the lidar nor radar provided a valid return), and when only the lidar detected cloud under **(b)** coupled (CBH-LCL < 125 m) and **(c)** decoupled (CBH-LCL > 125 m) conditions. LWP bins of  $20 \text{ g m}^{-2}$ .

[Title Page](#)[Abstract](#)[Introduction](#)[Conclusions](#)[References](#)[Tables](#)[Figures](#)[◀](#)[▶](#)[◀](#)[▶](#)[Back](#)[Close](#)[Full Screen / Esc](#)[Printer-friendly Version](#)[Interactive Discussion](#)

## Millimeter-wave stratocumulus LWP retrievals

P. Zuidema et al.

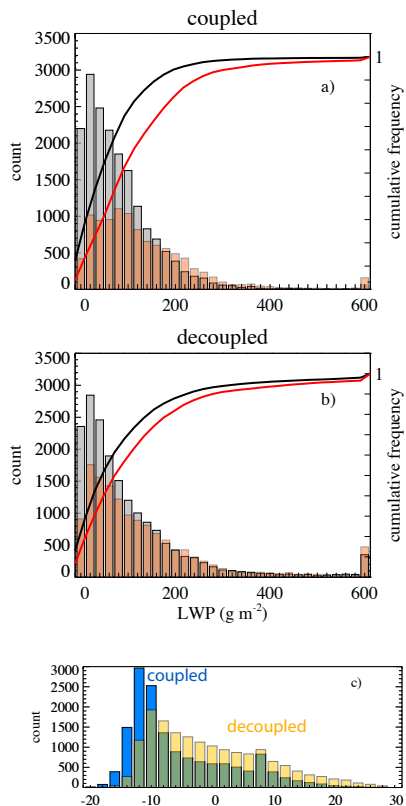


**Fig. 13.** Distributions of GVR-retrieved (black) and adiabatic (red) LWPs from the subcloud legs of thirteen research flights for **(a)** coupled (CB-LCL < 125 m) and **(b)** decoupled (CB-LCL > 125 m) conditions. LWP bins of  $20 \text{ g m}^{-2}$ , only samples with known cloud bases and lifting condensation levels were considered. **(c)** The count distributions of the column-maximum radar reflectivities for coupled and decoupled conditions.

Title Page

Abstract

Introduction

Conclusions

References

Tables

Figures

◀

▶

◀

▶

Back

Close

Full Screen / Esc

Printer-friendly Version

Interactive Discussion

